Resonant cavity enhanced photonic devices

Maciej Bugajski, Jan Muszalski, Bohdan Mroziewicz, Kazimierz Regiński, Tomasz J. Ochalski

Institute of Electron Technology, al. Lotników 32/46, 02–668 Warszawa, Poland.

In the present paper, we review our recent works on technology, basic physics and applications of one-dimensional photonic structures. We demonstrate spontaneous emission control in $In_xGa_{1-x}As$/GaAs planar microcavities with DBR reflectors. The room temperature emission in λ-sized cavities is enhanced in comparison with its free space value, while in $\lambda/2$-sized cavities suppression of spontaneous emission is observed. The characteristics of spontaneous emission in microcavities depend on the wavelength difference between the emitter and the cavity resonance. It has been shown that ideal tuning of the cavity can be achieved by adjusting sample temperature. In general, observed trends are in agreement with theoretical predictions. These changes to the spontaneous emission process directly affect vertical-cavity laser (VCSEL) properties. An increased coupling efficiency of spontaneous emission into the lasing mode is observed in VCSELs with λ-sized cavities. We demonstrate the operation of resonant-cavity light emitting diodes (RC LED) and optically pumped VCSELs developed recently at the Department of Physics and Technology of Low Dimensional Structures of the Institute of Electron Technology. The epitaxial growth issues, fabrication technology and basic characteristics of these devices are discussed.

1. Introduction

In recent years a number of optoelectronic devices employing microcavity structures were proposed. Such devices benefit from utilization of specific effects resulting from placing the active structure inside the Fabry–Perot type microcavity. The most notable examples of such devices are Vertical Cavity Surface Emitting Lasers (VCSEL) and Resonant Cavity Light Emitting Diodes (RC LED) realized in the early nineties [1]. The main advantages of resonant cavity LEDs over conventional devices are higher emission intensities, higher spectral purity and more directional emission patterns. On the other hand, VCSELs benefit from increased coupling of spontaneous emission into the laser mode and small size which enables dynamic single mode operation and large modulation bandwidth [2], [3]. Efficiency and high speed at low powers are of paramount importance for such applications of VCSELs as short-haul data communications, printing and optical switching. Planar technology and resulting manufacturability of VCSELs is an added value.

2. Distributed Bragg reflectors and microcavities

The laser cavity of a VCSEL is usually constructed normal to the substrate plane by stacking multilayer films including an active region, spacer and two dielectric mirrors.

Such a structure forms a one dimensional Fabry–Perot cavity resonator. A dielectric mirror can be formed with a periodic stack of quarter wavelength thick layers of alternating high and low refractive index material. Such a mirror is referred to as a distributed Bragg reflector (DBR). The dielectric layers can be semiconductor layers deposited via molecular beam epitaxy (MBE). The active region usually consists of a spacer layer of the thickness equal to integer multiple of the half wavelength and of one or several quantum wells (QWs). The quantum wells are typically situated at the antinodes of the standing wave pattern. Some of the attractive features of VCSELs are connected with the possibility of controlling the spontaneous emission (SE) in the microcavity structure, and in particular, with enhanced coupling of the spontaneous emission into the lasing mode [4].

The simplest form of an optical cavity consists of two coplanar mirrors separated by an optical length of either one wavelength (λ-type cavity) or one-half wavelength ($\lambda/2$-type cavity). Coplanar cavities are the simplest form of the optical microcavities. Their properties will be discussed below. We will start with discussing the properties of GaAs microcavities containing InGaAs quantum well placed in the middle of the cavity. The excitonic transitions in the quantum well are the source of spontaneous emission, which properties we want to analyze depending on the size of the cavity. The Bragg mirrors on both sides of the cavity are composed of an equal number of pairs of quarter-wavelength AlAs/GaAs layers, which makes them transparent to the radiation generated in the quantum well. What determines the spontaneous emission rate in such microcavities is the amplitude of the electric field of the standing-wave of the cavity mode at the location of quantum well. In a λ-cavity quantum well is located in the antinode of the cavity, whereas in a $\lambda/2$-cavity exciton dipole is located in the node of the cavity as shown in Fig. 1. These two distinctively
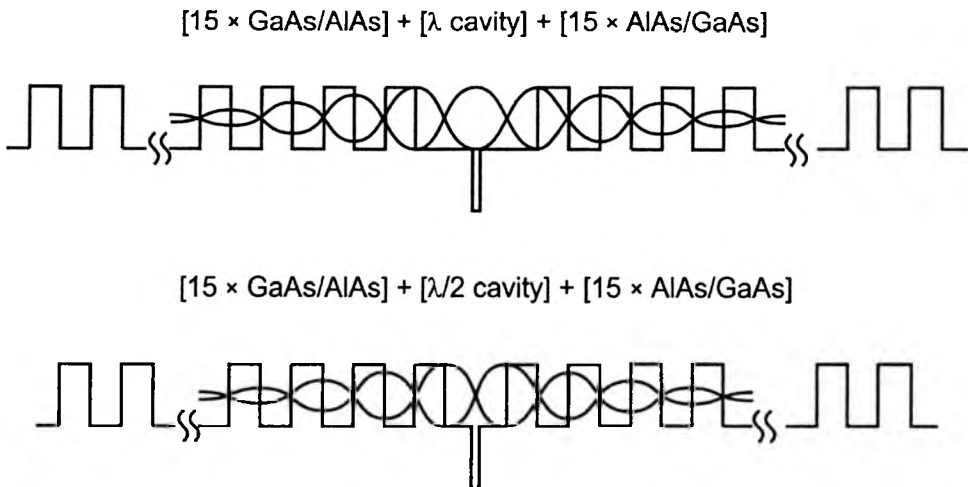
[15 × GaAs/AlAs] + [λ cavity] + [15 × AlAs/GaAs]

[15 × GaAs/AlAs] + [λ/2 cavity] + [15 × AlAs/GaAs]

Fig. 1. Schematic illustration of the band diagram of the λ-sized and $\lambda/2$-sized microcavities. Note the shape of the standing wave pattern in both cases.

different situations should reflect in spontaneous emission properties of the microcavities discussed.

The optimisation of microcavity requires proper tuning of the wavelength of radiation emitted from the active region, the peak reflectivity of DBRs, and the cavity resonance. This is the reason why the structure performance is very sensitive to variations in the thickness of layers and their composition. The wavelength of radiation from quantum well depends on both the composition and thickness. The spectral shape of the reflectivity of DBRs in the case of GaAs/AlAs reflectors depends on the layer thickness in the mirrors. Similarly, the position of the cavity resonance depends on the thickness of the spacer layers between the mirrors and the QW region and the phase of reflection from the mirrors. Thus, the optimum performance of the structure requires simultaneous alignment of all three features [5]. The goal in growing the mirrors for a VCSEL is to get layers that are approximately a quarter wavelength thick each and to get the reflection band centered at the right wavelength. If the layer thickness slightly differs from a quarter wavelength, it is not so important as long as the reflection band is situated in the right place. The position of the cavity resonance will ultimately determine the lasing wavelength. From theoretical considerations it follows that in a properly fabricated laser structure the wavelength of the reflectivity peak may be shifted by $\pm 2\%$, or each layer thickness may vary by $\pm 2\%$. It means that the accuracy of the control of gallium and aluminum fluxes during the MBE growth should be of the order of 2%.

The required accuracy can hardly be achieved without additional internal control in the MBE system. Thus, besides careful calibration of the growth rate and composition, some additional methods of internal control should be applied. The real time control of growing layers has been achieved in our case by applying pyrometric interferometry. This method allows continuous monitoring and readjustment of growth rate to maintain the given thickness of the layers [6], [7]. The advantage of the method is that it does not require any additional equipment, nor necessitates any modifications to MBE machine. It simply makes use of the already installed pyrometer and relies on the analysis of the intensity of infrared thermal radiation emitted by growing layers.

We have used a standard IRCON pyrometer to measure the temperature in the center of the substrate. This particular model is especially designed to measure the GaAs surface temperature by monitoring radiation emitted in a narrow range of wavelengths ($0.940\pm0.03\mu m$), which are shorter than the band edge of GaAs (but longer than $Al_xGa_{1-x}As$, $x > 0.25$) at temperatures which are of interest for MBE (400–750 °C). For these wavelengths the absorption coefficient is of the order of 10^4 cm^{-1}, so a 1 μm thick GaAs layer can still be considered as opaque, *i.e.*, the pyrometer registers radiation emitted by the surface of the structure but not the radiation emitted by the substrate heater.

These apparent temperature oscillations due to interference effects caused by refractive index steps at heterointerfaces are shown in Fig. 2 for the case of the growth of microcavity structure. The structure consists of two Bragg reflectors (15 pairs of quarter-wave AlAs and GaAs layers, $\lambda = 1000$ nm) separated by λ-sized cavity with

$In_{0.2}Ga_{0.8}As$ QW in the center. In this case, each layer of the Bragg reflector contributes new interfaces to the multiple internal reflections of radiation. As a result the amplitude of temperature oscillations has increased up to ~15 °C (*cf.* Fig. 2). This sudden change in the temperature readout at the AlAs/GaAs interfaces is caused by a change of thermal radiation background when the Ga and Al shutters are opened and closed, respectively. Analysing the data taken during the whole growth process one can notice that although the readout temperature changes drastically with time, the average temperature stays constant. This proves that substrate temperature control based on the thermocouple readout gives satisfactory results, although the real temperature value must be established in a different way. One can also notice that the shape of oscillations stabilises after the growth of approximately 8 pairs of AlAs/GaAs layers composing Bragg mirror. This proves that the pyrometer measures the radiation emitted from the top (~1 μm thick layer) of the structure as can be expected from simple analysis of the absorption of thermal radiation in the structure.

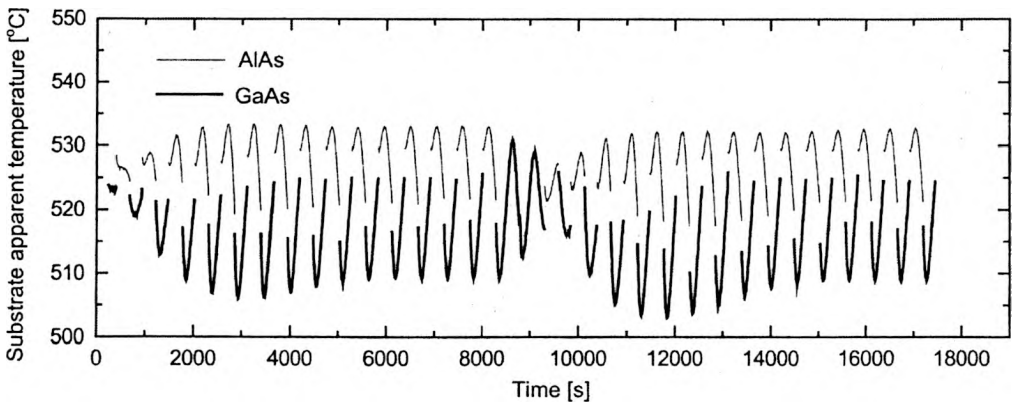Fig. 2. Pyrometer readout during the MBE growth of $In_{0.2}Ga_{0.8}As$/GaAs VCSEL structure.

The apparent temperature oscillations can be used to determine the thickness of layers which otherwise would be difficult to access. Since the actual phase of the interference signal depends on the thickness of the grown layer, they can be used to calibrate the growth rate. The growth rate G can be related to the oscillation period T by the relation

$$G = \left(\frac{1}{T}\right)\left(\frac{\lambda}{2n}\right)\cos\alpha \tag{1}$$

where λ is the pyrometer operating wavelength (0.940 μm), n – the refractive index of the layer at the growth temperature and α – the angle of incidence. Calibrating the

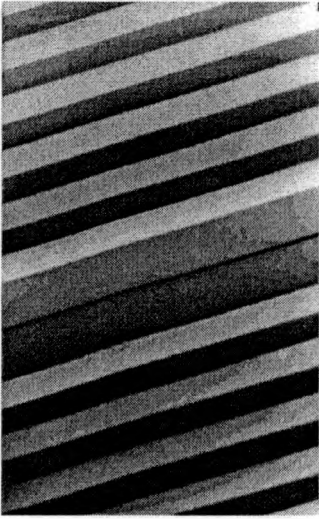Fig. 3. TEM pictures of λ-sized $In_{0.2}Ga_{0.8}As/GaAs$ planar microcavitiy. The structure has been grown by MBE at the Department of Physics and Technology of Low Dimensional Structures of the Institute of Electron Technology. The bright regions in the photograph refer to AlAs, the dark region refer to GaAs; the narrow dark line in the middle of the cavity refers to InGaAs QW.
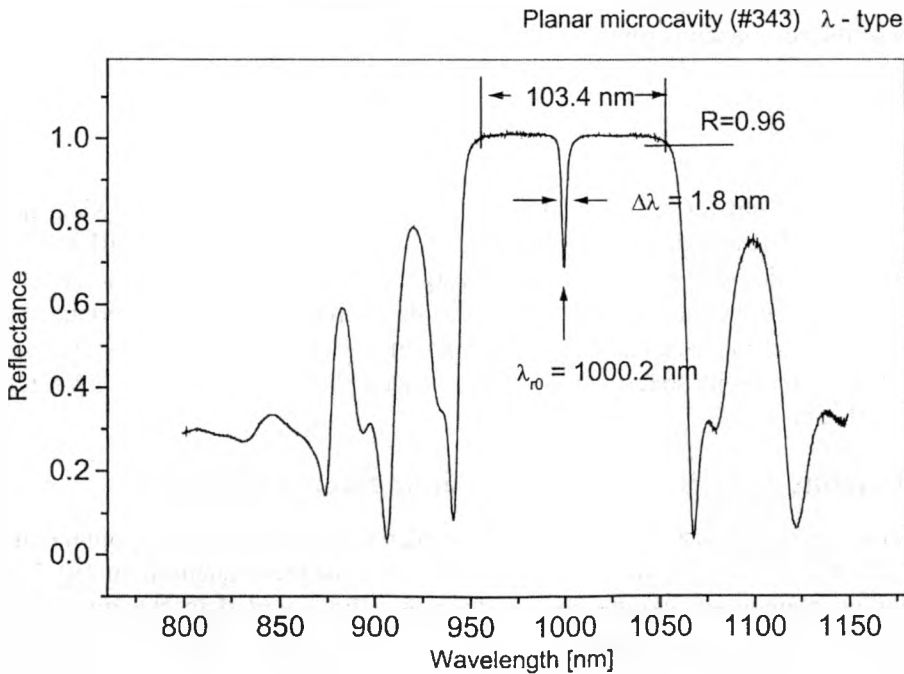

Fig. 4. Refelectance spectrum of λ-sized $In_{0.2}Ga_{0.8}As/GaAs$ planar microcavity, resonant at 1000 nm.

refractive index the pyrometric oscillations can later be used for the growth rate measurements over the thick layers, *i.e.*, verification of the group III flux stability. The accurate gallium flux control is also essential to maintain λ_{QW} within ±2 nm to assure matching with VCSEL cavity resonance. To achieve low threshold currents in VCSELs it is necessary to maintain the difference between these two below ~5 nm. Such strict requirements are difficult to fulfil unless some *in-situ* control technique is applied. Figure 3 shows the transmission electron microscope (TEM) picture of λ-sized, $In_{0.2}Ga_{0.8}As/GaAs$ planar microcavity grown with the aid of pyrometric interferometry. The measured reflectivity spectrum of microcavity considered is shown in Fig. 4. The width of the high reflectivity stop-band at normal incidence is roughly given by [8]

$$\Delta\lambda_{\text{stop-band}} = \frac{2\lambda_B \Delta n}{\pi n_{eff}} \qquad (2)$$

where Δn is the refractive index difference between the dielectric layers, n_{eff} – the effective refractive index of the mirror (arithmetic mean of the refractive indices in the stack) and λ_B – the Bragg wavelength. For AlAs/GaAs mirror, the stop-band predicted by Eq. (1) for $\lambda_B = 1000$ nm is 98.4 nm, which is in good agreement with 103.4 nm observed experimentally. The stop-band is flat and peak reflectivity is as expected theoretically for this type of reflector, *i.e.*, 0.979. Note also the accuracy in obtaining the resonance frequency, *i.e.*, 1000.2 nm vs. 1000 nm, which was attempted. The width of the resonance is given by the expression

$$\Delta\lambda = \frac{\lambda_B^2(1-R)}{2\pi L\sqrt{R}}, \qquad (3)$$

which leads to 0.97 nm for λ-sized cavity. Experimental value is almost twice that much, *i.e.*, 1.8 nm. The broadening of the resonance is mainly caused by the reflectivity measurement conditions. The probing beam divergence is the source of inhomogenous broadening of the reflectance dip. Estimations show that in order to produce the broadening observed the beam divergence of about 2.5° is enough. Cavity finesse, calculated from reflectivity spectra, is 277.7 for λ-sized cavity and 833.3 for $\lambda/2$-sized cavity ($\Delta\lambda = 1.2$ nm).

3. Spontaneous emission control in planar microcavities

In this section, we will discuss the effect of a planar microcavity on spontaneous emission. We will basically follow our earlier treatment of these phenomena [9]. Let us consider an elementary excitation (exciton) in solid coupled to the quantized radiation field. The coupling can be described by a perturbation term in the exciton-field Hamiltonian

$$V = e\mathbf{dE}. \qquad (4)$$

The exciton is in initial (excited) state and drops into the final (ground) state emitting a photon of energy $\eta\omega$. The rate of spontaneous emission γ_{sp} is given by the Fermi golden rule

$$\gamma_{sp} = \frac{2\pi}{\eta}|\langle i|e\mathbf{d}\mathbf{E}|f\rangle|^2\rho(\omega) \tag{5}$$

where $e\mathbf{d}$ is the (vector) dipole moment, $\mathbf{E}$ – the electric field at the location of the exciton dipole, and $\rho(\omega)$ – the density of optical modes per unit energy at angular frequency ω. It is clear from Eq. (5) that spontaneous emission rate can be altered either by modifying the mode density, or by modyfing the electric field at the location of the exciton dipole. Both the mode density and the electric field can be modified in a microcavity the size of which is properly adjusted. To observe cavity related effects, the field does not have to be confined in all three dimensions. One dimensional microcavities already give sizeable effects, although their strength scales up with the degree of confinement. Inside the cavity, the electromagnetic field forms a standing wave which meets the resonance condition, namely the round trip phase shift equal to integer multiple of 2π, as in the Fabry–Perot resonators made of metallic mirrors.

Reflectance, photoluminescence perpendicular to the Bragg reflector (PL), and photoluminescence from the edge of the structure (PL in plane) of λ-sized $In_{0.2}Ga_{0.8}As/GaAs$ planar microcavity, resonant at 1000 nm are shown in Fig. 5. The photoluminescence signal from the edge of the structure can be regarded as a reference spontaneous emission unaffected by the cavity. In the direction perpendicular to the
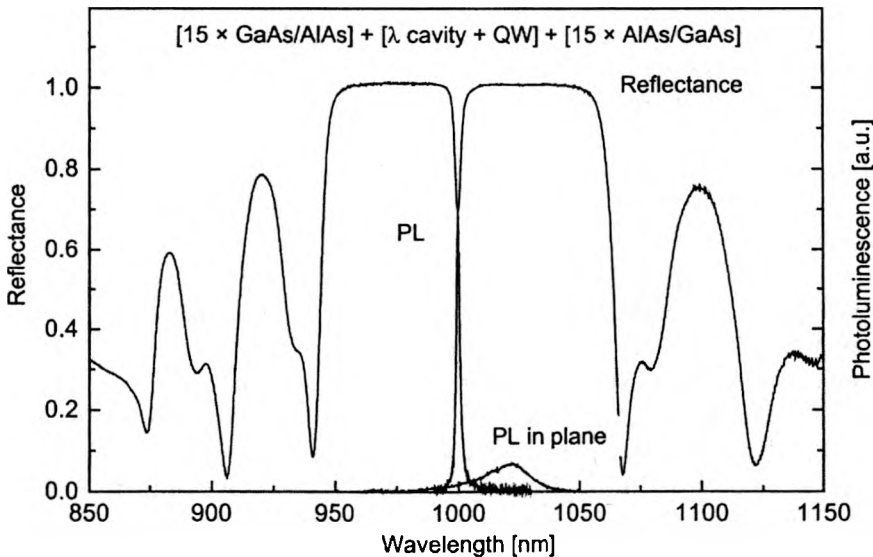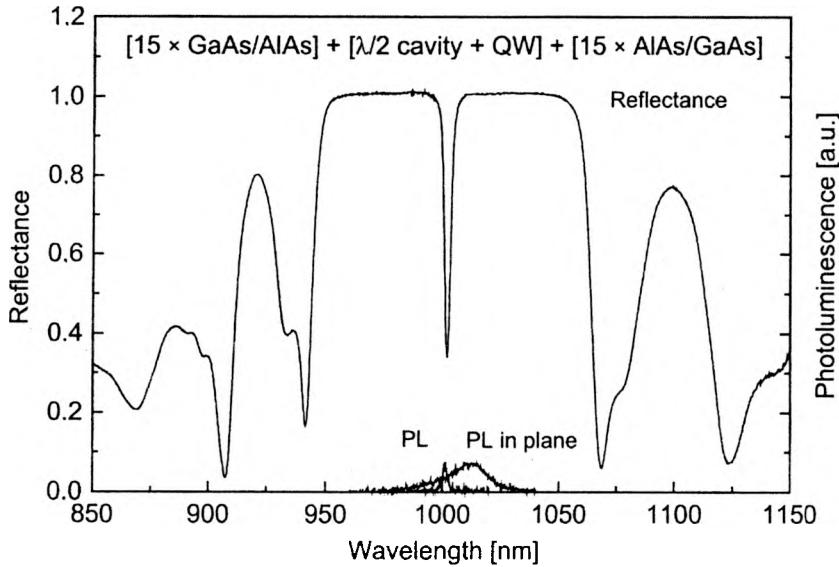

Fig. 5. Reflectance, photoluminescence perpendicular to the Bragg reflector, and photoluminescence from the edge of the structure (PL in plane) of λ-sized $In_{0.2}Ga_{0.8}As/GaAs$ planar microcavity, resonant at 1000 nm.

Fig. 6. Reflectance, photoluminescence perpendicular to the Bragg reflector and photoluminescence from the edge of the structure (PL in plane) of $\lambda/2$-sized $In_{0.2}Ga_{0.8}As/GaAs$ planar microcavity, resonant at 1000 nm.

cavity plane the PL signal is concentrated in a narrow line forced by cavity resonance and its intensity increases roughly by a factor of 10 (the integrated intensity of PL line increases 1.9 times). The characteristics of spontaneous emission in microcavities depend on the wavelength difference between the emitter and the cavity resonance. By lowering sample temperature it is possible to shift QW PL line to higher energies, while the position of the cavity resonance remains practically unaffected. In the case of λ-sized cavity discussed, temperature tuning produces further increase of PL signal by another factor of 10, which leads to total enhancement of PL signal by the microcavity by about 100. This is to be compared with calculated cavity enhancement factor equal to 190.

Another type of cavity is the $\lambda/2$-sized microcavity in which QW positioned in the center of the spacer is located at the node of standing wave pattern of the cavity mode. Reflectance, photoluminescence perpendicular to the Bragg reflector, and photoluminescence from the edge of the structure (PL in plane) of $\lambda/2$-sized $In_{0.2}Ga_{0.8}As/GaAs$ planar microcavity, resonant at 1000 nm are shown in Fig. 6. As might be expected, this cavity effectively quenches PL signal (the ratio of integrated intensity of PL perpendicular to PL in plane signal is 1/12). The fact that there is still some PL emitted from the cavity is due to two factors. The first one is that we collect PL signal from small solid angle around direction perpendicular to the cavity, the second is that QW might be slightly off the center with respect to intended position and consequently exciton dipole interacts with a nonzero field amplitude. Nevertheless the PL quenching by $\lambda/2$-sized cavity is beyond any doubt. This is an important result

because it once again proves that spontaneous emission is not an inherent property of emitter but it is indeed a stimulated emission, stimulated by vacuum field fluctuations of the electromagnetic field in the cavity.

4. Vertical cavity surface emitting laser

Vertical cavity lasers are significantly more difficult to fabricate than their edge-emitting counterparts, but the rapid evolution of their performance in recent years paved the way to many applications of them. The VCSEL structures discussed in this paper were grown by molecular beam epitaxy (MBE) on (100) oriented GaAs substrates using Riber 32P solid source reactor. The structures consisted of two Bragg mirrors; the lower formed by 24.5 pairs of quarter-wavelength AlAs/GaAs layers and the upper formed by 14.5 pairs of quarter-wavelength AlAs/GaAs layers. The estimated reflectivity of the lower mirror was equal to 99.7%, whereas that of the upper mirror was equal to 97%. In between the mirrors GaAs microcavity of the thickness 2λ, containing 3×3 InGaAs quantum wells located at the antinodes of standing wave pattern of the laser mode, was placed (see Fig. 7). The structure was intended for optical pumping experiments and as such was undoped. In real structures of electrically
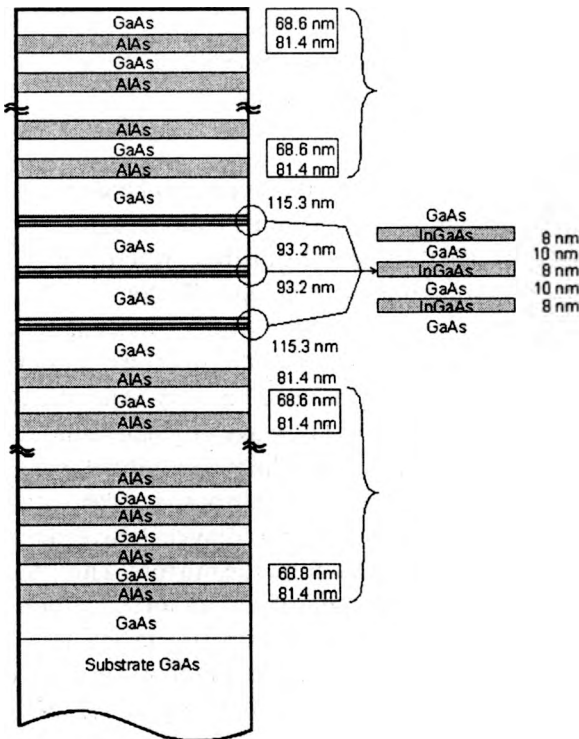

Fig. 7. Schematic VCSEL structure with 3×3 InGaAs QW active region designed for operation at 1 μm at $T = 300$ K.
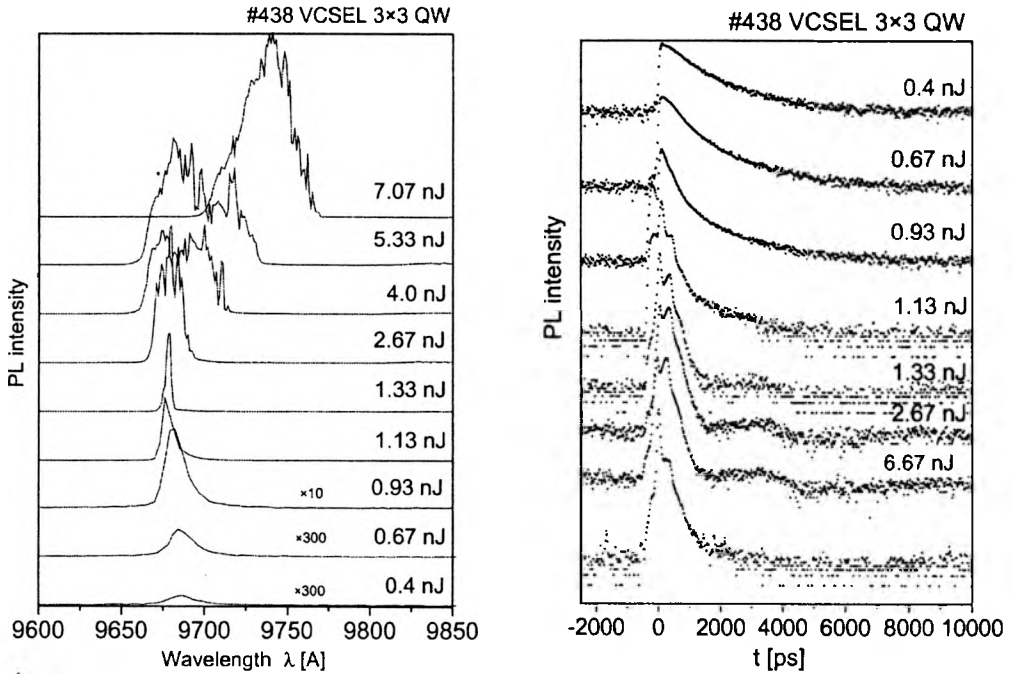
Fig. 8. Emission spectra of 3×3 QW InGaAs VCSEL structure under optical pumping.

Fig. 9. Emission decay for optically pumped 3×3 QW InGaAs VCSEL structure.

pumped VCSELs the Bragg reflectors to act as carrier emitters have to be doped to n- and p-type conductivity going from the bottom to the top of the structure. In electrically pumped VCSEL the light is extracted through the substrate, whereas in the case of optically pumped device it emerges through the top Bragg reflector.

The optimization of the microcavity requires proper tuning of the wavelength of radiation emitted from the active region, the peak reflectivity of the structure, and the cavity resonance. It is the reason why the VCSEL performance is very sensitive to variations in thickness of the layers and their composition. The wavelength of radiation from the QW depends on both the composition and thickness. The reflectivity of Bragg reflectors depends on the thickness of individual layers in the mirrors. Similarly, the position of cavity resonance depends on the thickness of the spacer layers between the mirrors and the QWs region and the phase of the reflection from the mirrors. Thus, the optimal growth of the structure requires simultaneous alignment of all three features. However, some variation of those parameters can be tolerated depending on how much variation in threshold and efficiency is acceptable for the device. The required accuracy can hardly be achieved without additional non-standard internal control in the MBE system. Thus, besides careful calibration of the growth rate and composition, applying such methods as, for example interference pyrometry or laser reflectometry, is essential for maintaining proper growth conditions.

The VCSEL structures were optically excited by high power, pulse laser at room temperature. The transverse extent of the optical cavity was defined by the diameter of the laser beam and did not exceed 100 μm. The spectral shape and the intensity of VCSEL emission and decay of the emission as a function of pump pulse energy were measured. The results of measurements are shown in Fig. 8 and Fig. 9. At low excitation densities a regular photoluminescence signal was observed. For higher excitations we have observed a clear threshold behaviour and rapid increase of the emission intensity accompanied by the characteristic line narrowing. For very high pumping pulse energies (≥ 2.67 nJ) emission starts to behave unstable and shifts to lower energies, which is the result of heating. The plot of emission intensity from VCSEL structure vs. pump pulse energy is shown in Fig. 10. The threshold occurs at pump pulse energy of about 0.7 nJ. At the same time a marked decrease of the carrier lifetime, from about 700 ps to 50 ps, *i.e.*, more than one order of magnitude, is observed (Fig. 11). This is a characteristic behaviour for the transition from spontaneous to stimulated emission, and because it coincides with other characteristic features such as threshold in the emission intensity characteristics and line narrowing it can be regarded as a final proof of the laser action in the VCSEL structures under investigation.

To produce devices suitable for electrical pumping, besides doping emitters, one has to form appropriate electrical contacts and define dimensions of pumped region in transverse directions which can be done by proton implantation or etching a suitable
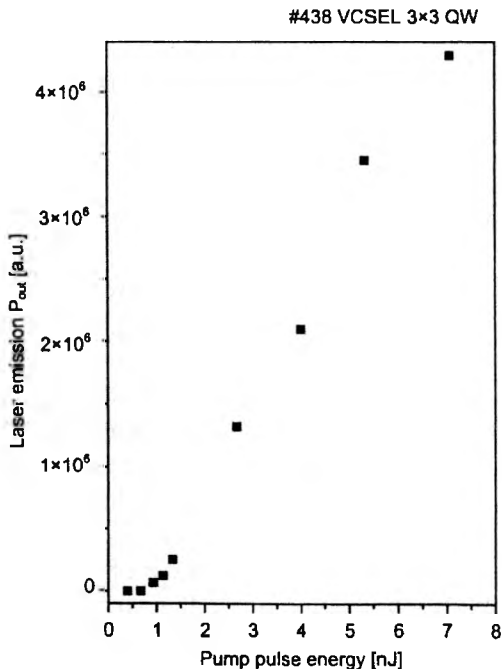

Fig. 10. Emission intensity vs. pumping pulse energy for 3×3 QW InGaAs VCSEL structure.
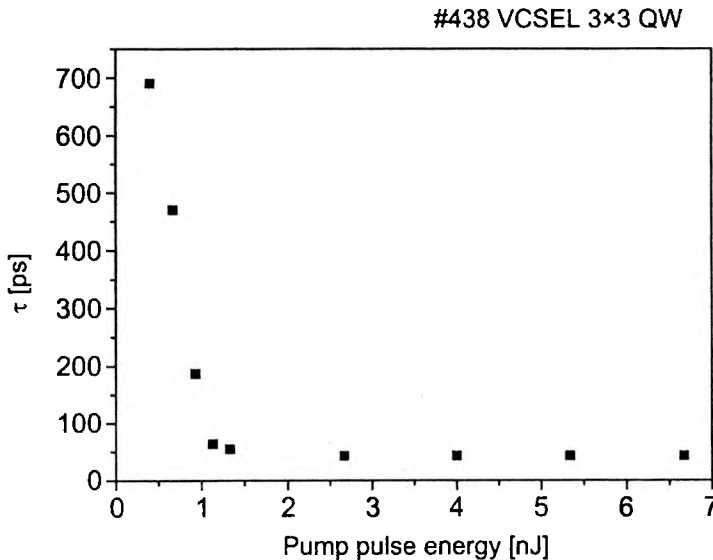
#438 VCSEL 3×3 QW

Fig. 11. Carrier lifetime vs. pumping pulse energy for 3×3 QW InGaAs VCSEL structure.

post followed by polymide isolation. The biggest obstacle on the way to fabricate efficient, low threshold lasers is electrical resistivity of Bragg reflectors (especially that of p-type reflector) contributing to the series resistance of the device. This resistance can be reduced by appropriate profiling of the interfaces in the Bragg reflectors. Preliminary results of technological experiments carried out in our laboratory show that both step grading and digital alloy grading of the AlAs/GaAs and GaAs/AlAs interfaces in the reflectors, combined with δ -doping, lead to a substantial decrease of resistivity. The voltage at the forward biased VCSEL drops from 5–6 V for abrupt profile reflectors to about 2.5 V for graded interface and δ -doped reflectors. The last value is roughly twice the value of the turn on voltage for simple p-n junction GaAs diode without reflectors.

The vertical cavity laser is in principle a zero threshold laser [10]. In conventional, edge emitting laser, only a small portion of the spontaneous emission couples into a laser mode. The rest is lost to free-space modes, which radiate in all directions. In 3D confined vertical cavity laser with wavelength size cavity in which only one optical mode exists, all spontaneous and stimulated emission is coupled to that mode and no clear distinction between spontaneous and stimulated regimes exists. In planar 1D cavities due to the lack of transverse confinement there is still a threshold of laser action observed but it is substantially reduced. While in conventional lasers spontaneous emission to the laser mode coupling factor β is of the order of 10^{-5} and for ideal zero threshold laser β should equal 1, we have obtained $\beta = 10^{-3}$ for our weakly confined VCSELs; *i.e.*, 100 times threshold reduction. Even though this is still far from the theoretical limit it is a significant improvement compared to edge emitting lasers.

5. Resonant cavity light emitting diodes

The RC LED operation relies on enhanced spontaneous emission occurring in microcavity structures. The main advantages of resonant-cavity diodes over conventional LEDs are: higher emission intensities, narrower emission lines and more directional emission pattern, which makes RC LEDs an attractive alternative for lasers in many applications. The structure of RC LED resembles that of the VCSEL, the main
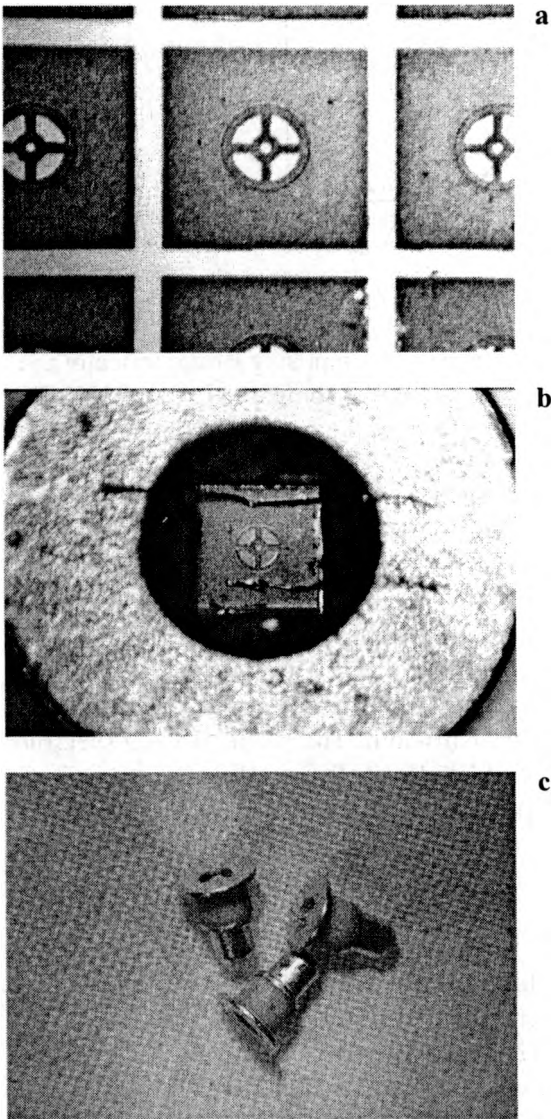

Fig. 12. RC LED structures on a wafer, before separating them into individual chips (**a**), view of the chip mounted inside the case (**b**), assembled diodes (**c**).
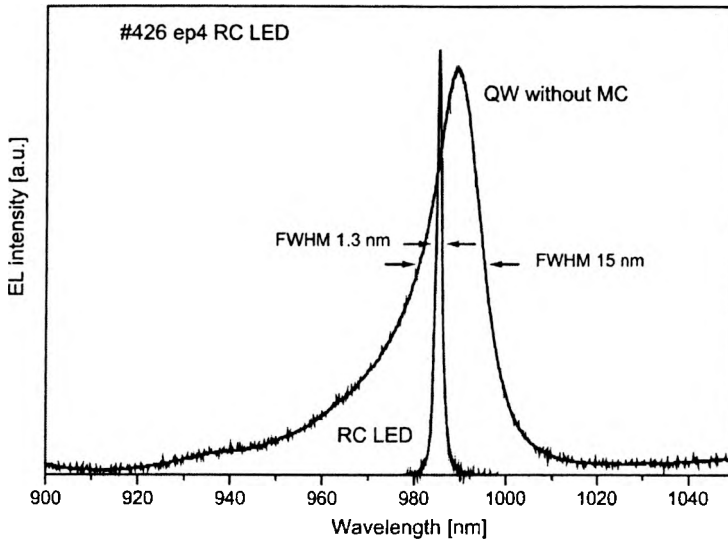
Fig.13. Emission spectrum of RC LED compared to conventional LED.

difference being the smaller number of pairs of layers composing Bragg reflectors. As a result, the reflectivity and the cavity finesse Q are lower compared to typical VCSEL values. The cavity is defined by two Bragg reflectors, the active region is composed of two InGaAs QW each 80 A thick, separated by 100 A Gaas barrier. The light from the diode is extracted through the openings in the upper Cr–Pt contact. The bottom Au–Ge contact (to the n-type substrate) forms a solid circle. The diode structure is formed by conventional photolitography and metallization. The devices were designed for the emission at $\lambda = 1$ μm. Figure 12 shows diode structures on a wafer, before separating them into individual chips (**a**), view of the chip mounted inside the case (**b**) and assembled diodes (**c**). The emission properties of RC LED and conventional LED are shown in Fig. 13. Compared to classical LED the spectrum of RC LED is concentrated into a narrow line with 1.3 nm halfwidth. The shape of LED spectrum reflects thermal distribution of electrons and holes in the conduction and valence bands. On the other hand, the RC LED spectrum is determined mainly by the cavity resonance; its width decreases with an increase of cavity finesse and the intensity increase reflects the on-axis cavity enhancement. The figure of merit of LED used in optical fiber communication systems is the photon flux density emitted from the diode at a given current, for a given wavelength. Since the optical power coupled into a fiber is directly proportional to the photon flux density, the RC LEDs are particularly suitable for fiber link applications. Another favourable RC LED property is in this case its emission characteristic directionality. The higher spectral purity of RC LED reduces also chromatic dispersion in optical fiber communications. The RC LEDs can indeed be very bright. In principle, the enhancement of the spontaneous emission inside the cavity and emission through one of the mirrors out of the cavity can be very different. For cavities of very high finesse, which are typical for VCSELs the overall emission

out of the cavity can decrease (in the limit of very high reflectivity $R = 100\%$ the emission out of the cavity becomes zero). At moderate values of the finesse, which are characteristic for RC LEDs the spontaneous emission both inside and out of the cavity can be enhanced even by more than an order of magnitude [11].

6. Conclusions

We have demonstrated that for the reproducible growth of microcavities and in particular vertical cavity surface emitting lasers by MBE, the growth rate of the individual layers has to be controlled with accuracy better than 2%. To achieve this level of process control, a real time monitoring of the growth is required. In this work, we also report on the apparent substrate temperature oscillations observed by infrared pyrometry during the MBE growth of multilayer laser structures and demonstrate their usefulness in process control. The phase information and the period of oscillations provide information on the actual growth rate, whereas the mean value of the pyrometer readout correlates with the true substrate temperature. The interference pyrometry offers a convenient alternative to standard laser reflectometry when it is necessary to control growth rate of thick layers with high precission. Using the above method we have grown a number of microcavities and VCSEL structures with precisely tailored Bragg reflector characteristics and cavity resonance tuned to the center of DBR stop-band an quantum well emission wavelength.

Spontaneous emission control has been achieved in $In_xGa_{1-x}As/GaAs$ planar microcavities with DBR reflectors. The room temperature emission in λ-sized cavities is enhanced compared to its free space value while in $\lambda/2$-sized cavities suppression of spontaneous emission is observed. The characteristics of spontaneous emission in microcavities depend on the wavelength difference between the emitter and the cavity resonance. It has been shown that ideal tuning of the cavity can be achieved by adjusting sample temperature. In general, observed trends are in agreement with theoretical predictions. These changes to the spontaneous emission process directly affect VCSEL properties. An increased coupling efficiency of spontaneous emission into the lasing mode is observed in VCSELs with λ-sized cavities.

We also report laser action in optically pumped InGaAs/GaAs VCSELs operating at 980 nm at room temperature. Works are in progress on Bragg reflector optimization with respect to electrical resistivity and on device fabrication issues, which are expected to render electrically pumped devices. So far we have developed resonant-cavity light emitting diodes with very good emission charactristics. RC LEDs proved to be more tolerant to the epitaxial growth parameters and device fabrication procedures. As relatively robust devices they are less sensitive to manufacturing challenges typical for VCSEL and seem to have great potential for commercialization. The problems which are still to be solved, before the technology can be regarded as mature, are wafer uniformity, yield and reliability of the devices. Nevertheless, even at the moment there is no doubt that resonant cavity enhanced devices (emitters) and VCSELs will have a profound impact on optoelectronic and photonic systems.

References

[1] UNLU M. S., STRITE S., J. Appl. Phys. **78** (1995), 607.

[2] CHANG-HASNAIN C.J. *Vertical-cavity surface-emitting lasers*, [In] G.P.Agrawal [Ed.], *Semiconductor Lasers; Past, Present, and Future*, AIP Press, Woodbury, 1995, pp. 145–180.

[3] COLDREN L. A., HEGBLOM E. R., AKULOVA Y. A., *et al.*, *VCSELs in 98: What we have and what we can expect*, [In] K. D. Choquette, R. A. Morgan [Eds], *Vertical-Cavity Surface-Emitting Lasers II*, Proc. SPIE **3286** (1998), 2.

[4] BABA T., HAMANO T., KOYAMA F., IGA K., IEEE J. Quantum Electron. **27** (1991), 1347.

[5] GEELS R. S. *Vertical-cavity surface-emitting lasers: Design, fabrication and characterization*, PhD Thesis, University of California, Santa Barbara 1991.

[6] MUSZALSKI T., Thin Solid Films **367** (2000), 299.

[7] REGIŃSKI K., MUSZALSKI J., BUGAJSKI M., *et al.*, Thin Solid Films **367** (2000), 290.

[8] BJORK G., YAMAMOTO Y. *Spontaneous emission in dielectric planar microcavities*, [In] Yokoyama H., Ujihara K. [Eds.], *Spontaneous Emission and Laser Oscillation in Microcavities*, CRC Press, Boca Raton 1995, pp. 189–235.

[9] OCHALSKI T., MUSZALSKI J., ZBROSZCZYK M., *et al.*, *Spontaneous emission control in $In_xGa_{1-x}As/GaAs$ planar microcavities with DBR reflectors*, NATO Science Series, 3. High Technology, Vol. 81, *Optical Properties of Semiconductor Nanostructures*, M. L. Sadowski *et al.* [Eds.], pp. 201–210 (2000).

[10] YOKOYAMA, H., Science **256** (1992), 66.

[11] HUNT N. E. J., SCHUBERT E. F., LOGAN R. A., ZYDZIK G. J., Appl. Phys. Lett. **60** (1992), 921.